Part I

Grown-In Defects in Bulk Crystals

SYSTEMATIC ANALYSES OF PRACTICAL PROBLEMS RELATED TO DEFECTS AND METALLIC IMPURITIES IN SILICON

Y.KITAGAWARA*,H.TAKENO**,S.TOBE**, Y.HAYAMIZU**,T.KOIDE**,T.TAKENAKA*
* SEH Shirakawa R&D Center, Shin-Etsu Handotai Co., Ltd., 150 Oh-hira, Odakura, Nishigo, Nishi-Shirakawa, Fukushima 961-8061, Japan, kitagawara@seh.co.jp
**SEH Isobe R&D Center, Shin-Etsu Handotai Co., Ltd., 2-13-1 Isobe, Annaka, Gunma-ken 379-0196, Japan

ABSTRACT

Systematic approaches are introduced for (i) oxygen precipitation behavior, which is important for internal gettering, and (ii) segregation induced gettering behaviors of p/p^+ epitaxial wafers and Poly-Si Back Seal (PBS) wafers. (i) Oxygen precipitation behavior during a whole sequence of a thermal process is predicted by a practical computer simulation technique involving a novel empirical function. The predicted oxygen precipitation behavior agrees with the corresponding experimental results reasonably well. (ii) For a systematic description of Fe segregation gettering, explicit expressions of the Fe segregation coefficients are obtained as functions of temperature and time. Using the determined expressions of the segregation coefficients and introducing diffusion dynamics, one can predict [Fe] behavior as a function of process time during a whole sequence of a thermal process. For both behaviors of (i) oxygen precipitation and (ii) segregation induced gettering, experimentally observed characteristics of a high-temperature process and a low-temperature process are well understood by aids of those simulations. (iii) For a high-sensitivity detection of an important heavy metal impurity Cu, we present a novel bulk impurity collection technique using a room-temperature Cu drift phenomenon accelerated by Corona charge showering on a Si wafer surface.

INTRODUCTION

As ULSI electronic device becomes more integrated and miniaturized, near surface quality of the Si substrate wafer is demanded to be high with extremely low contaminant concentration and with very low defect density. Even though use of epitaxial wafers or low defect density Czochralski (CZ) wafers significantly reduce device failures induced by grown-in crystal defects [1], it is still required to reduce and control heavy metal impurities in the surface and near-surface regions of the Si wafers. Metal impurity gettering technology is quite important to control near-surface contamination and to suppress defect generation in the device active region during a ULSI fabrication process. It is thus desirable to understand the gettering behaviors systematically and to predict defect generation and the gettering ability for any given thermal process. Even before the device thermal process, very fast diffusing element like Cu can possibly contaminate the starting Si wafer at a relatively low temperature or even at a room temperature [2]. From this aspect, development of highly sensitive metal detection and its elimination is important.

In this paper, we discuss (i) oxygen precipitation behaviors which are important for internal gettering and (ii) segregation induced Fe gettering behaviors of p/p^+ epitaxial wafers and Poly-Si Back Seal (PBS) wafers. The experimentally observed behaviors of a high-temperature CMOS process and a low-temperature process are well characterized by the aid of our numerical simulation

Mat. Res. Soc. Symp. Proc. Vol. 510 © 1998 Materials Research Society

techniques for those problems. In addition, we present (iii) a high-sensitivity bulk Cu detection technique which utilizes electrical Cu drift phenomenon accelerated by room-temperature Corona charge showering on a Si wafer surface.

EXPERIMENTS

Oxygen Precipitation Behaviors

Samples investigated are 5-20 Ωcm p-type CZ wafers, p/p^- epitaxial wafers with substrate resistivities 5-20 Ωcm, 0.012-0.020 Ωcm p^+ CZ wafers, and p/p^+ epitaxial wafers. For the p-type CZ and p/p^- epi wafers, interstitial oxygen concentration [Oi] and precipitated oxygen content Δ[Oi] are measured by an ordinary infrared absorption method [3]. Bulk microdefect (BMD) densities were evaluated by Secco preferential etching method [4]. For the p^+ CZ and p/p^+ epi wafers, oxygen concentrations were measured by a Gas-Fusion method [5], precipitated oxygen contents were measured by an X-ray diffraction method [6], and BMD densities were evaluated by Wright preferential etching method [7] or an infrared laser scattering tomography [8]. The above oxygen concentrations and the precipitated oxygen contents are calibrated on the JEIDA scale [3].

The oxygen precipitation behaviors were studied for three different thermal processes. One is a two-step process consisting of an 800° C step for 4h in nitrogen ambient and the following 1000° C step for 16h in dry oxygen ambient. Another is a high-temperature CMOS process simulation described in Fig. 1. The other is a low-temperature thermal simulation described in Fig. 2. Comparative study on the precipitation characteristics of the high-temperature process and those of the low-temperature process is presented for the p/p^+ epi wafers.

Segregation Induced Fe Gettering Behaviors

To determine Fe segregation coefficient as a function of gettering temperature in p/p^+ epi wafers, 10 Ωcm p-type epi-layers were deposited on highly boron-doped p^+ substrates with resistivities between 0.005 and 0.07 Ωcm. Thickness of the epi-layer and that of the substrate were 10 and 675 μm respectively. Oxygen concentration of the p^+ substrate was 14ppma-JEIDA as determined by a gas fusion method [5]. These sample epi-wafers were contaminated with $1 \times 10^{12} cm^{-2}$ Fe by a spin coating method [9], then heat-treated at 1000°C for 1h in nitrogen ambient for the iron in-diffusion. After the contamination, the Fe gettering heat treatments were carried out at temperatures between 600 to 950°C. The heat treatment time was set to be long enough so as to make the Fe impurities

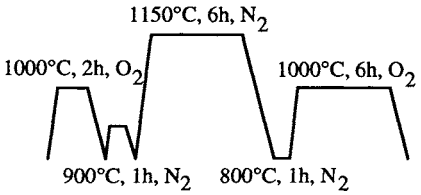

Fig. 1. High-temperature CMOS simulation

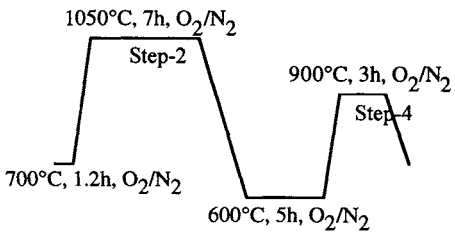

Fig. 2. Low-temperature process simulation.

diffuse deep enough about 1mm. The samples were then quenched in water. The Fe concentration at the epi near-surface was evaluated by deep level transient spectroscopy (DLTS) as a sum of both interstitial iron concentration and iron-boron pair concentration.

To obtain gettering temperature dependence of near-surface [Fe] in a PBS wafer, Fe in-diffusion was carried out at 1000°C for 5h for 10 Ωcm p-type FZ-Si wafers with 1.1μm-thick polysilicon films on the back surfaces. The Fe gettering heat treatments were carried out at temperatures between 550 and 800°C, then cooled down rapidly. The Fe diffusion length was kept about 780μm at each gettering temperature. The [Fe] was evaluated by the DLTS and the SPV method [10]. In addition, the PBS grain growth rate and the solid phase epitaxy rate were evaluated by transmission electron microscope observation in a temperature range between 800 and 1150°C.

High-Sensitivity Bulk Cu Detection

Samples were 10 Ωcm p-type CZ-Si wafers, which were intentionally Cu-contaminated by chemomechanical polish using slurry containing low-level Cu [2]. "Low-level" contamination was made by using slurry containing 50ppb of copper nitrate. "high-level" contamination was made by using slurry containing 150ppb of copper nitrate. The control wafer with no intentional contamination was also prepared.

For a high-sensitivity bulk Cu detection, we utilized a room-temperature Cu drift phenomenon accelerated by Corona negative charge showering on a Si wafer surface. Negative Corona ion showering was applied on the p-type CZ-Si wafer surface with the native oxide. Continuous Corona ion shower with 1.3×10^{-9} C cm^{-2} s^{-1} was applied for 0 ~ 6 h. Concentration of the surface Cu collected by the Corona shower was measured by the total reflection X-ray fluorescence spectroscopy (TXRF) using Technos TREX 610.

RESULTS AND DISCUSSION

Oxygen Precipitation Behaviors

Internal gettering by oxygen precipitation is well known to be relaxation type [12]. This type of gettering caused by controlled oxygen precipitation is quite important even in a p/p^+ epi-wafer with strong "boron gettering" capability [13]. Thus we should be able to predict and to optimize the oxygen precipitation characteristics of an arbitrary thermal process of our interest. Recently, Takeno *et al.* have developed a practical computer simulation technique to predict the oxygen precipitation behaviors [14,15]. It is based on the Fokker-Planck equation for the oxygen precipitation, where a novel empirical factor is introduced in the initial and the boundary conditions so as to make up an incomplete assumption of a conventional homogeneous nucleation process. Furthermore, an experimentally measured thermal history during a crystal growth process is taken into consideration as the very first step of the crystal thermal history, which is followed by a device process thermal simulation. The calculated values predict reasonably well the experimental results of Δ[Oi] and the oxide precipitate density for various thermal processes without using adjustable parameters.

In Fig. 3, we show results of the numerical calculations of the precipitated oxygen contents for a two-step process consisting of an 800° C step for 4h in nitrogen ambient and the following 1000° C step for 16h in dry oxygen ambient. The calculated results are shown by the solid lines together with

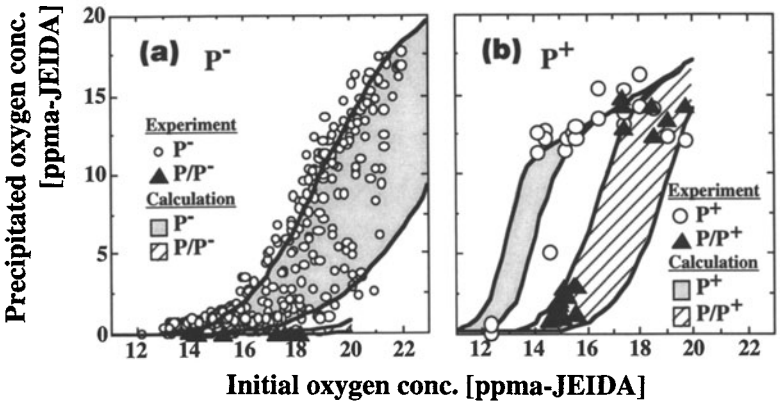

Fig. 3. Dependence of precipitated oxygen content on oxygen concentration for a two-step heat process, 800°C 4h + 1000°C 16h. (a) is for p- substrates and p/p- epi wafers. (b) is for p+ substrates and p/p+ epi wafers. Upper curve of the numerical calculation is for head-sections of the crystal ingots. Lower curve is for the tail-sections.

the experimental data points. The upper curve is for the head-section of the crystal ingot which experienced the longest CZ growth thermal history within the ingot. The lower curve is for the tail-section with the shortest CZ thermal history. The region between the two curves is a distribution range of the precipitated oxygen contents for samples between the head-section and the tail-section. A region of the experimental data distribution agrees well with the computer simulated precipitation region for the ingot. From Figs. 3 (a) and (b), we understand the characteristic oxygen precipitation behaviors to be as follows. The epi wafers p/p^- and p/p^+ have less tendency to generate oxygen precipitation than the corresponding p^- and p^+ substrates with no epi-deposition process at 1150°C in this case. It implies that many of the oxygen precipitation nuclei produced during the Czochralski crystal pulling were annihilated at the high-temperature epi deposition process. Especially in case of the p/p^- epi-wafers, the oxygen precipitation hardly occurs even at a very high oxygen concentration > 18 ppma. Therefore one should be very careful about a possible weak internal guttering capability for metal contamination in case of the p/p^- epi-wafers. On the other hand, the p/p^+ epi-wafers have much higher tendency to generate oxygen precipitation than the p/p^- epi-wafers. Thus the p/p^+ wafers are considered to be better suited for a process which requires an internal gettering ability induced by the oxygen precipitation.

We now study characteristics of oxygen precipitation behaviors of a high-temperature CMOS process described in Fig. 1 and a low-temperature process described in Fig. 2. Resistivity and oxygen content of the p^+ substrate are 0.015Ωcm and 14ppma, respectively. Epi process is held at 1130°C for 5min. With the aid of the computer simulation, the precipitate density is evaluated as a function of the precipitate radius. Fig. 4 shows the size distribution after the high-temperature CMOS process described in Fig. 1. On the other hand, for the low-temperature process of Fig. 2, the density-size distribution right after an intermediate step-2 is given by the histogram in Fig. 5 (a) and that after the final step-4 is given in Fig. 5 (b). In the size distribution of Fig. 4 for the high-temperature process and that in Fig. 5 (a) for the process intermediate stage, all the oxygen precipitates are larger than 20nm in the radii. However, at the final stage of the low-temperature process, one observes the characteristic small-size distribution of oxygen precipitates with radii < 20nm. The small-size precipitate distribution is created during the low-temperature stages below

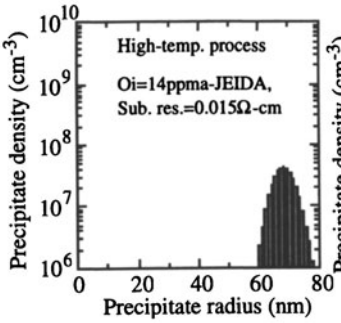

Fig. 4. Density-size distribution after a high-temperature CMOS simulation.

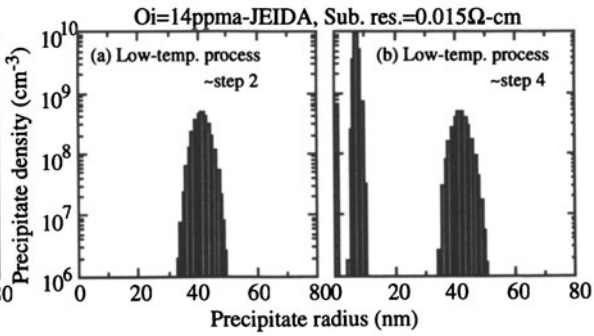

Fig. 5. (a) Calculated density-size distribution after intermediate step 2 and (b) that after final step 4 of a low-temperature process.

900°C after the step-2.

To understand more sequentially, we have calculated precipitate density as a function of the process time. Figures 6 and 7 are for the high-temperature CMOS process and the low-temperature process, respectively. The solid curve shows the density of all the oxygen precipitates with the radii ≥ 0.2nm. The dotted curve shows the density of the relatively large precipitates with the radii ≥ 20nm. As shown in Fig. 6 for the high-temperature CMOS process, it is characteristic that the total oxygen precipitate density is determined at the very first step of the process simulation. Only the precipitate size growth takes place predominantly at the early part of the high-temperature CMOS process. No significant precipitate nucleation occurs during the CMOS process sequence. On the other hand, as we observe in Fig. 7 for the low-temperature process, oxygen precipitate nucleation and growth occur at the late stages below 900°C especially after the intermediate step-2. This is indeed a basic reason to observe a characteristic small-size precipitate distribution of radius < 20nm in Fig. 5 (b). The precipitate growth takes place predominantly at the steps higher than 1000°C for both the high-temperature and the low-temperature processes.

To compare the results of the computer simulation with the corresponding experimental data, we show in Figs. 8 and 9 the relations between precipitate density and oxygen concentration after the high-temperature process and the low-temperature process, respectively. In case of Fig. 9 for the low-temperature process, the numerical calculations of the precipitates with radii ≥ 0.2nm are drawn by the solid curve and the corresponding experimental data are plotted by the circular dots.

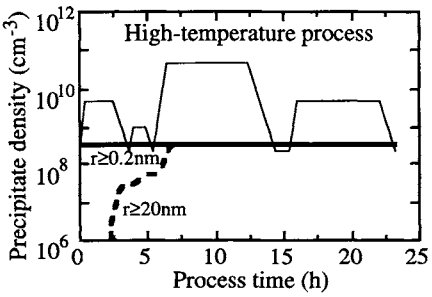

Fig. 6. Calculated precipitate density variation during a high-temperature CMOS simulation.

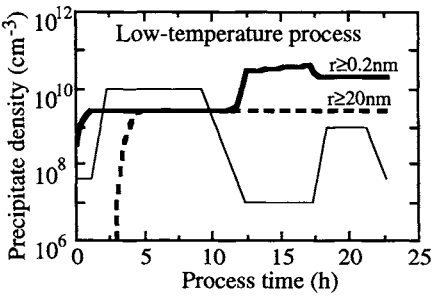

Fig. 7. Calculated precipitate density variation during a low-temperature process simulation.

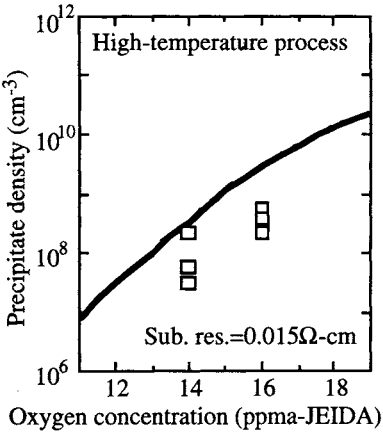

Fig. 8. Precipitate density versus oxygen concentration for a high-temperature process. Solid curve is for calculation. Square dots are for experiments

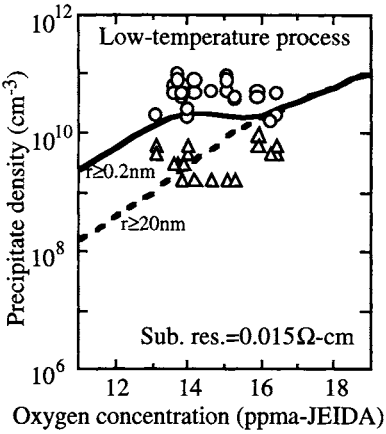

Fig. 9. Precipitate density versus oxygen concentration for a low-temperature process. Curves are for calculations. Circular dots are total etch pit densities. Triangular dots are large-size etch pit densities.

For the radii ≥ 20nm, the calculations are described by the dotted curve and the experimental data are plotted by the triangular dots. Strictly speaking, the experimental data in Fig. 9 are not necessarily for the size ranges ≥ 0.2nm and ≥ 20nm, but we have simply plotted the circular dots counting all the etching pits observed and the square dots only counting the pits with the sizes larger than 2μm after Wright etching [7]. On the other hand, for the high-temperature CMOS process, all the etching pits were large-size, and the experimental data are plotted by the square dots together with the calculated curve in Fig. 8. In this case, small-size precipitates with radii < 20nm do not exist in practice. Even though we cannot make strict comparison between calculation and experiment because of lack of an adequate small-size precipitate observation technique, numerical simulations in Figs. 9 and 10 represent reasonably well the experimental characteristics of the high-temperature CMOS and the low-temperature process. The existence of the small-size precipitate distribution is considered to be an important characteristic feature of a low-temperature process. We also emphasize that this type of computer simulation is an advantageous tool to predict and to optimize the oxygen precipitation characteristics of an arbitrary unknown device fabrication process.

Segregation Induced Fe Gettering Behaviors

Fe gettering by a highly boron-doped p^+ substrate is known to be segregation-induced type [16]. When one knows a precise expression of the segregation coefficient as a function of temperature, it becomes possible to predict the Fe gettering behavior. The first task is to determine the temperature dependence of the Fe segregation coefficient experimentally. In a segregation mechanism, the equilibrium iron concentration C_1 in a p-type epitaxial-layer is expressed as [17,18]

$$C_1 = \frac{C_0}{1 + \frac{W_2}{W_1 + W_2} A \exp(\frac{E}{kT})}, \qquad (1)$$

where C_0 is the initial contamination level when Fe impurities are distributed uniformly throughout the wafer. W_1 and W_2 are the thicknesses of the epi-layer and the p^+ substrate, respectively. E and A are values specific to metal impurity and gettering method. E is named as "activation energy" of the gettering reaction. The quantity A is described as $(N/N_{Si})A'$, where N is the gettering site density, N_{Si} is the silicon atomic density, and A' is a constant related to an entropy term of a gettering reaction. In previous studies of Fe gettering in p/p^+ wafers, values of the activation energy E and the constant A have not been accurately evaluated yet. This makes difficult to deduce the Fe concentration quantitatively. Therefore we determine the activation energy and the constant A precisely for the Fe gettering in p/p^+ epi-wafers. In order to determine the two unknown constants A and E, Eq.1 is transformed into a logarithmic form

$$\ln\left[\frac{C_1 W_2}{(C_0 - C_1)(W_1 + W_2)}\right] = \ln\left(\frac{1}{A}\right) - \frac{E}{kT}. \qquad (2)$$

When the left-hand side values are plotted versus $1/T$ in an Arrhenius type plot, the slope of the straight line gives the activation energy E and the intercept gives the constant A.

We show in Fig. 10 the experimentally observed gettering temperature dependence of Fe concentration C_1 in p-type epi-layer for the three substrates with different resistivities. The Fe concentration decreases with lowering the gettering temperature and with the increase of doped boron concentration. It is found that the Fe gettering efficiency becomes higher with increase of doped boron concentration in the substrate. The dotted line in Fig.10 shows the iron solubility in silicon [19]. Left-side of the solubility line means a supersaturated region of iron, and right-side is an unsaturated region. Since the iron gettering occurs even in the unsaturated region, the gettering mechanism is segregation type. This result agrees with the conclusions in previous works. Using Eq. 2, Fig. 10 can be transformed into Fig. 11 in a form of Arrhenius plot. From the slope in Fig. 11, the activation energy is determined to be 0.68eV which is very close to the binding energy 0.65eV of iron-boron complex [20]. Consequently, Fe gettering by the heavy boron doping is considered to be

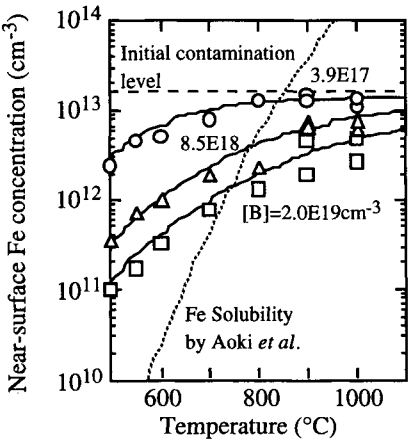

Fig. 10. Dependence of residual Fe concentration in epi-layer on gettering temperature.

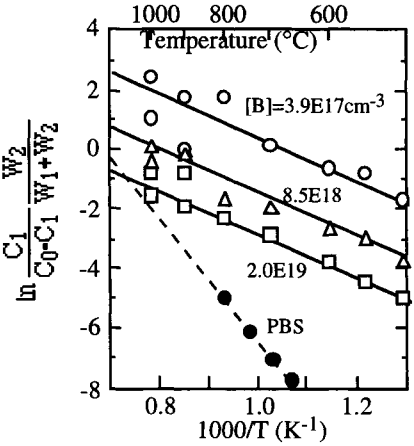

Fig. 11. Temperature dependence of equilibrium constants for gettering reactions.

related to formation of Fe-B complex in a heavily boron-doped substrate. From the intercept values ln(1/*A*) in Fig. 11, we understand that the *A* value increases with the doped boron concentration in the substrate. Relation between *A* and the boron concentration in the substrate is shown in Fig. 12. A very good linearity shows that *A* is proportional to the boron concentration. This is expressed as $A = 3.7 \times 10^{-22}$ cm^3 [B]. These experimentally determined values are now usable for a numerical Fe gettering simulation.

During a device thermal simulation, however, the metallic impurity is not always in an equilibrium situation. In such a non-equilibrium state, we need to introduce diffusion dynamics in the numerical gettering simulation. Here we use the Fick's second law written as

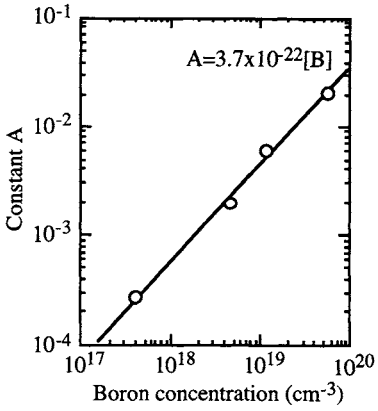

Fig. 12. Relation between the constant A and boron concentration in the substrate.

$$\frac{\partial C}{\partial t} = D\frac{\partial^2 C}{\partial x^2}, \qquad (3)$$

where *t* is time, *x* is depth from surface, and *D* is impurity diffusion coefficient. During the whole sequence of a thermal process, we assume that the impurity ratio of the substrate concentration C_2 to the epi-layer concentration C_1 at the substrate/epi interface is described in accordance with the relation in Eq. 1. Namely, at any moment during the process sequence, we assume that the segregation ratio C_2/C_1 at the substrate/epi interface is fixed immediately at the corresponding equilibrium segregation coefficient $1 + A\ exp(E/kT)$, even when the regions except the interface are not in an equilibrium situations at that moment. Numerically solving Eq. 3 with this assumption, the Fe gettering behavior of a p/p$^+$ epi-wafer is simulated as shown in Fig. 13 for a high-temperature CMOS process. The near-surface Fe concentration is calculated as a function of process time. The Fe gettering becomes efficient during a relatively low temperature step and during a wafer cooling process. On the other hand, when a higher temperature step comes after the lower temperature step, the gettering effect diminishes because of the impurity re-emission from the p$^+$ substrate region to the epi-layer. Consequently the temperature of a very final heat step or the final cooling rate is crucially important for the gettering efficiency determination. Figure 13 also shows that the Fe gettering capability becomes higher with the increase of boron concentration in the substrates. In the figure, the substrate boron concentrations of the p/p$^+$ and the p/p^{++} epi-wafers are 4.6×10^{18} and 1.1×10^{19} cm^{-3}, respectively.

We now investigate another important segregation-induced gettering by the polysilicon back-seal (PBS) in a similar way. In this case the temperature dependence of the Fe segregation coefficient was already studied in detail by Hayamizu *etal* [21]. The Arrhenius plot for the PBS gettering is also shown in Fig. 11 together with the results for the boron gettering. From the slope of the dotted line in Fig. 11, the activation energy *E* for the PBS gettering is 1.8eV which is much higher than the 0.68eV value for the boron gettering. In case of the PBS gettering, we also take into account the degradation of the PBS texture by the polysilicon grain growth and the solid phase epitaxy (SPE)